TRANSACTIONS ON ELECTRICAL AND ELECTRONIC MATERIALS
Vol. 18, No. 6, pp. 364-369, December 25, 2017

Regular Paper

pISSN: 1229-7607 eISSN: 2092-7592
DOI: https://doi.org/10.4313/TEEM.2017.18.6.364
OAK Central: http://central.oak.go.kr

Microwave Sol-Gel Derived $NaGd(MoO_4)_2$:Ho^{3+}/Yb^{3+} Phosphors and Their Upconversion Photoluminescence Properties

Chang Sung Lim†
Department of Advanced Materials Science & Engineering, Hanseo University, Seosan 31962, Korea

Received February 15, 2016; Accepted July 26, 2017

Double molybdate $NaGd_{1-x}(MoO_4)_2$:Ho^{3+}/Yb^{3+} phosphors with proper doping concentrations of Ho^{3+} and Yb^{3+} (x = Ho^{3+} + Yb^{3+}, Ho^{3+} = 0 and 0.05, and Yb^{3+} = 0, 0.35, 0.40, 0.45, and 0.50) were successfully synthesized using the microwave sol-gel method. Well-crystallized particles formed after heat-treatment at 800°C for 16 h showed fine and homogeneous morphologies with particle sizes of 1~3 μm. The spectroscopic properties were examined using photoluminescence emission and Raman spectroscopy. Under excitation at 980 nm, the upconversion doped samples exhibited strong yellow emissions, from the combination of strong emission bands at 545 nm and 655 nm in the green and red spectral regions, respectively. The strong 545 nm emission band in the green region corresponded to the $^5S_2/^5F_4 \rightarrow {}^5I_8$ transition in the Ho^{3+} ions, while the strong 655 nm band in the red region appeared because of the $^5F_5 \rightarrow {}^5I_8$ transition in the Ho^{3+} ions. The pump power dependence and the Commission Internationale de L'Eclairage chromaticity of the upconversion emission intensity were evaluated in detail.

Keywords : Microwave sol-gel, Spectroscopy, Double molybdate, Yellow

1. INTRODUCTION

Recently, the design and synthesis of rare-earth-activated photoluminescent particles have drawn considerable attention for their use in applications, such as fluorescent lamps, cathode ray tubes, solid-state lasers, amplifiers for fiber optics communication and novel optoelectronic devices, owing to their ability to overcome many of the current limitations of the traditional photoluminescent materials [1-3]. Scheelite-structured compounds belonging to the molybdate family have attracted considerable attention because of their spectroscopic characteristics and excellent upconversion (UC) photoluminescence properties [4,5]. Most of $NaLn(MoO_4)_2$ (Ln = La^{3+}, Gd^{3+}, Y^{3+}) compounds possess tetragonal scheelite structure with the space group $I4_{1/a}$, and belong to the family of double molybdates compounds. The $NaLn(MoO_4)_2$ transforms to a stable tetragonal scheelite structure from the monoclinic structure. Ho^{3+} and Yb^{3+} ions can partially substitute the trivalent rare-earth ions in the tetragonal phase. These ions are effectively doped into the crystal lattices of the tetragonal phase, because their radii are similar to those of the trivalent rare-earth ions, which results in excellent UC photoluminescence properties [6-8]. Among the rare-earth ions, the Ho^{3+} ion is suitable for converting infrared to visible light through the UC process owing to its appropriate electronic energy level configuration. The co-doped Yb^{3+} and Ho^{3+} ions can remarkably enhance the UC efficiency for the shift from infrared to visible light, because of the efficiency of the energy transfer from Yb^{3+} to Ho^{3+}. The Yb^{3+} ion, as a sensitizer, can be dramatically excited by the incident light source energy. This energy is transferred to the activator from which radiation can be emitted. The Ho^{3+} ion activator acts as the luminescence center of the UC particles, while the sensitizer enhances the UC luminescence efficiency [9-11].

For the preparation of the double molybdate $NaLn(MoO_4)_2$, several techniques have been developed via specific preparation processes, such as solid-state reactions [12-15], sol-gel method [16,17], Czochralski method [18-21], hydrothermal method [22-26], microwave-assisted hydrothermal method [27], and pulse laser deposition [28]. For applying the UC photoluminescence in products, features such as homogeneous UC particle-size distribution and morphology need to be defined well. Compared to the usual

† Author to whom all correspondence should be addressed:
E-mail: cslim@hanseo.ac.kr

methods, microwave synthesis has the advantages of very short reaction time, small particle size, narrow particle size distribution, and high purity of the final polycrystalline samples. Microwave energy is delivered to the material surface by radiation and/or convection heating, which heat energy is transferred to the bulk of the material via conduction [29-31]. It is a cost-effective method that provides high homogeneity and is easy to scale-up, and it is emerging as a viable alternative approach for the quick synthesis of high-quality luminescent materials. In this study, $NaGd_{1-x}(MoO_4)_2$:Ho^{3+}/Yb^{3+} phosphors with proper doping concentrations of Ho^{3+} and Yb^{3+} (x = Ho^{3+} + Yb^{3+}, Ho^{3+} = 0 and 0.05, and Yb^{3+} = 0, 0.35, 0.40, 0.45 and 0.50) were successfully prepared using the microwave sol-gel method, followed by heat treatment. The synthesized particles were characterized by X-ray diffraction (XRD) and scanning electron microscopy (SEM). The pump power dependence and the Commission Internationale de L'Eclairage (CIE) chromaticity of the UC emission intensity were evaluated in detail. The spectroscopic properties were examined comparatively using photoluminescence (PL) emission and Raman spectroscopy.

2. EXPERIMENTS

In this study, precise amounts of $Na_2MoO_4{\cdot}2H_2O$ (99%, Sigma-Aldrich, USA), $Gd(NO_3)_3{\cdot}6H_2O$ (99%, Sigma-Aldrich, USA), $(NH_4)_6Mo_7O_{24}{\cdot}4H_2O$ (99%, Alfa Aesar, USA), $Ho(NO_3)_3{\cdot}5H_2O$ (99.9%, Sigma-Aldrich, USA), $Yb(NO_3)_3{\cdot}5H_2O$ (99.9%, Sigma-Aldrich, USA), citric acid (99.5%, Daejung Chemicals, Korea), NH_4OH (A.R.), ethylene glycol (A.R.) and distilled water were used to prepare $NaGd(MoO_4)_2$, $NaGd_{0.6}(MoO_4)_2$:$Ho_{0.05}Yb_{0.35}$, $NaGd_{0.55}(MoO_4)_2$:$Ho_{0.05}Yb_{0.40}$, $NaGd_{0.50}(MoO_4)_2$:$Ho_{0.05}Yb_{0.45}$, and $NaGd_{0.45}(MoO_4)_2$:$Ho_{0.05}Yb_{0.50}$ compounds with the correct doping concentrations of Ho^{3+} and Yb^{3+} (Ho^{3+} = 0 and 0.05, and Yb^{3+}= 0, 0.35, 0.40, 0.45 and 0.50). To prepare the compounds $Na_2MoO_4{\cdot}2H_2O$ and $(NH_4)_6Mo_7O_{24}{\cdot}4H_2O$ were dissolved in 20 mL of ethylene glycol and 80 mL of 5M NH_4OH under vigorous stirring and heating. Subsequently, $Gd(NO_3)_3{\cdot}6H_2O$ with $Ho(NO_3)_3{\cdot}5H_2O$, $Yb(NO_3)_3{\cdot}5H_2O$ and citric acid (the molar ratio of citric acid to the total metal ions was 2:1) were dissolved in 100 mL of distilled water under vigorous stirring and heating. Then, the solutions were mixed together vigorously and heated at 80~100℃. Finally, highly transparent solutions were obtained and adjusted to pHs of 7-8 by the addition of NH_4OH or citric acid. The transparent solutions were placed in a microwave oven operating at a frequency 2.45 GHz with a maximum output power of 1,250 W for 30 min. The working cycle of the microwave reaction was controlled very precisely using a regime of 40 s ON and 20 s OFF for 15 min, followed by further treatment with 30 s ON and 30 s OFF for 15 min. The samples were treated with ultrasonic radiation for 10 min to produce a light-yellowish transparent sol. After this, the light-yellowish transparent sol was dried at 120℃ in a dry oven to obtain black dried gels. The black dried gels were ground and heat-treated at 800℃ for 16 h at 100℃ intervals between 600~800℃. Finally, white particles were obtained for pure $NaGd(MoO_4)_2$ and pink particles were obtained for the doped compositions.

The phase composition of the synthesized particles were identified using XRD (D/MAX 2200, Rigaku, Japan). The microstructure and surface morphologies of the synthesized particles were observed using SEM (JSM-5600, JEOL, Japan). The PL spectra were recorded using a spectrophotometer (Perkin Elmer LS55, UK) at room temperature. The pump power dependence of the UC emission intensity was measured at levels of working power from 20 to 110 mW. The Raman spectra measurements were performed using a LabRam Aramis (Horiba Jobin-Yvon, France) with a spectral resolution of 2 cm^{-1}. The 514.5 nm line of an Ar ion laser was used as an excitation source; the power on the samples was kept at the 0.5 mW level to avoid the decomposition of the sample.

3. RESULTS AND DISCUSSION

Figure 1 shows the XRD patterns of the samples. Figure 1(a) shows the JCPDS 25-0828 pattern of $NaGd(MoO_4)_2$. Figures 1(b)~(f) show the XRD patterns of the synthesized particles pure $NaGd(MoO_4)_2$, $NaGd_{0.60}(MoO_4)_2$:$Ho_{0.05}Yb_{0.35}$, $NaGd_{0.55}(MoO_4)_2$:$Ho_{0.05}Yb_{0.40}$, $NaGd_{0.50}(MoO_4)_2$:$Ho_{0.05}Yb_{0.45}$, and $NaGd_{0.45}(MoO_4)_2$:$Ho_{0.05}Yb_{0.50}$ respectively. It is possible to assign almost all indexed XRD peaks to pure tetragonal phases, which is more and less consistent with the standard data of $NaGd(MoO_4)_2$ (JCPDS 25-0828). $NaGd(MoO_4)_2$, as a member of the double molybdate family has a scheelite structure with lattice constants of a = 5.235 Å and c = 11.538 Å [21], which is tetragonal with the space group $I4_{1/a}$. It can be observed, that the diffraction peaks of the doped samples of Figs. 1(c)~(f) shift slightly to the high angle compared to that of the pure sample of Fig. 1(b). In the crystal structure of $NaGd_{1-x}(MoO_4)_2$, the Gd^{3+} ion site is supposed to be occupied by Ho^{3+} and Yb^{3+} ions with fixed occupations according to the nominal chemical formulas. The defined crystal structure contains MoO_4 tetrahedrons coordinated by four (Gd/Ho/Yb)O_8 square antiprisms through the common O ions. In the doped crystals, the unit-cell shrinkage results from the substitution of the Gd^{3+} ions by the Ho^{3+} and Yb^{3+} ions. It is assumed that the radii of Ho^{3+} (R = 1.015 Å) and Yb^{3+} (R = 0.985 Å) are smaller than that of Gd^{3+} (R = 1.053 Å), when the coordination number is CN = 8 [32]. Consequently, it should be emphasized that the Ho^{3+} and Yb^{3+} ions can be effectively doped in the $NaGd_{1-x}(MoO_4)_2$ lattice by the partial substitution of the Gd^{3+} sites, which leads to the unit-cell shrinkage caused by the similar radii of Gd^{3+} and by the partial substitution of Ho^{3+} and Yb^{3+} while maintaining the tetragonal structure of $NaGd_{1-x}(MoO_4)_2$. Post heat-treatment plays an important role in attempting to establish a well-defined crystallized morphology. To achieve a well-defined crystalline morphology, the phases must be heat treated at 800℃ for 16 h. It is assumed that the doping concentrations of Ho^{3+}/Yb^{3+} have a suitable effect on the crystalline cell volume maintaining the original structure of the $NaGd(MoO_4)_2$.

Figures 2(a)~(d) present the SEM images of the synthesized $NaGd_{0.60}(MoO_4)_2$:$Ho_{0.05}Yb_{0.35}$, $NaGd_{0.55}(MoO_4)_2$:$Ho_{0.05}Yb_{0.40}$, $NaGd_{0.50}(MoO_4)_2$:$Ho_{0.05}Yb_{0.45}$, and $NaGd_{0.45}(MoO_4)_2$:$Ho_{0.05}Yb_{0.50}$ particles, respectively. The as-synthesized samples are well crystallized with fine and homogeneous morphologies and particle sizes in range of 1~3 μm. The samples show no discrepancy in terms of morphological features, and the agglomerated particles are

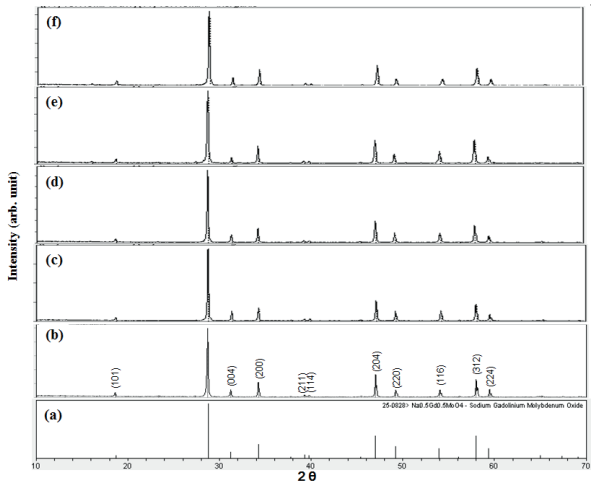

Fig. 1. X-ray diffraction patterns: (a) JCPDS 25-0828 pattern of $NaGd(MoO_4)_2$; XRD patterns of-, the synthesized (b) pure $NaGd(MoO_4)_2$, (c) $NaGd_{0.60}(MoO_4)_2$:$Ho_{0.05}Yb_{0.35}$, (d) $NaGd_{0.55}(MoO_4)_2$:$Ho_{0.05}Yb_{0.40}$, (e) $NaGd_{0.50}(MoO_4)_2$:$Ho_{0.05}Yb_{0.45}$, and (f) $NaGd_{0.45}(MoO_4)_2$:$Ho_{0.05}Yb_{0.50}$ particles.

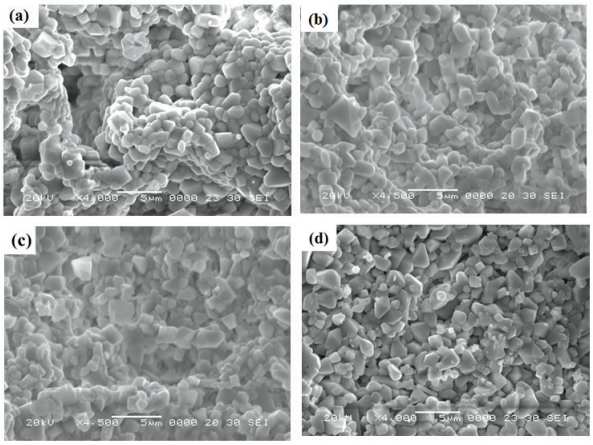

Fig. 2. Scanning electron microscopy images of the synthesized (a) $NaGd_{0.60}(MoO_4)_2$:$Ho_{0.05}Yb_{0.35}$, (b) $NaGd_{0.55}(MoO_4)_2$:$Ho_{0.05}Yb_{0.40}$, (c) $NaGd_{0.50}(MoO_4)_2$:$Ho_{0.05}Yb_{0.45}$, and (d) $NaGd_{0.45}(MoO_4)_2$:$Ho_{0.05}Yb_{0.50}$ particles.

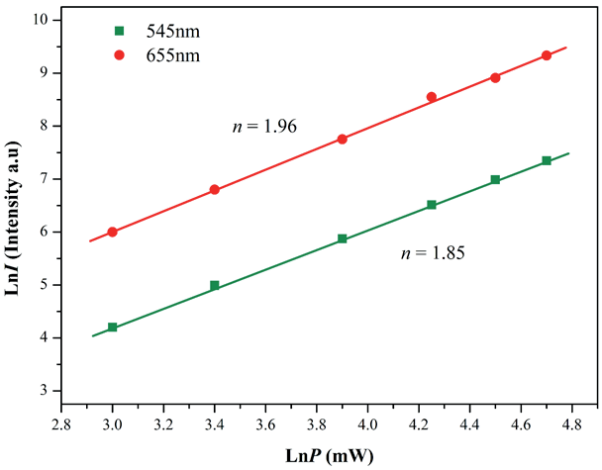

Fig. 4. Logarithmic scale dependence of the upconversion emission intensity on the pump power in the range of 20 to 110 mW at 545 and 655 nm in the $NaGd_{0.50}(MoO_4)_2$:$Ho_{0.05}Yb_{0.45}$ sample.

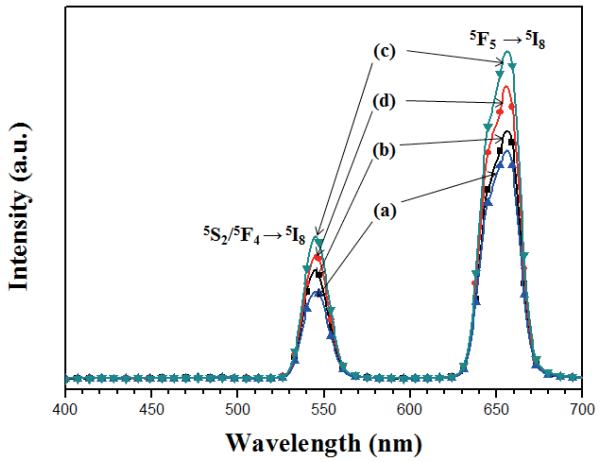

Fig. 3. The upconversion photoluminescence emission spectra of (a) $NaGd_{0.60}(MoO_4)_2$:$Ho_{0.05}Yb_{0.35}$, (b) $NaGd_{0.55}(MoO_4)_2$:$Ho_{0.05}Yb_{0.40}$, (c) $NaGd_{0.50}(MoO_4)_2$:$Ho_{0.05}Yb_{0.45}$, and (d) $NaGd_{0.45}(MoO_4)_2$:$Ho_{0.05}Yb_{0.50}$ particles excited under 980 nm at room temperature.

induced by the atom inter-diffusions among the grains. It should be noted that the doping concentrations for Ho^{3+} and Yb^{3+} have no effect on the morphological feature. The microwave sol-gel method for double molybdates provides the energy to synthesize the bulk of the material uniformly, so that fine particles with controlled morphologies are fabricated in a short period. The method is a cost-effective way to fabricate highly homogeneous products with easy scale-ups and is a viable alternative for the rapid synthesis of UC particles. This suggests that the microwave sol-gel route is suitable for the creation of homogeneous $NaGd_{1-x}(MoO_4)_2$:Ho^{3+}/Yb^{3+} crystallites.

Figures 3(a)~(d) shows the UC emission spectra of $NaGd_{0.60}(MoO_4)_2$: $Ho_{0.05}Yb_{0.35}$, $NaGd_{0.55}(MoO_4)_2$:$Ho_{0.05}Yb_{0.40}$, $NaGd_{0.50}(MoO_4)_2$:$Ho_{0.05}Yb_{0.45}$, and $NaGd_{0.45}(MoO_4)_2$:$Ho_{0.05}Yb_{0.50}$ particles, respectively, excited under 980 nm at room temperature. The doped samples exhibit strong yellow emissions based on the combination of strong emission bands at 545 nm and 655 nm in the green and red spectral regions, respectively. The strong 545 nm emission band in the green region corresponds to the $^5S_2/^5F_4 \rightarrow {}^5I_8$ transition in Ho^{3+} ions, while the strong 655 nm emission band in the red region is due to the $^5F_5 \rightarrow {}^5I_8$ transition in the Ho^{3+} ions. The Ho^{3+} ion activator acts as the luminescence center of these UC particles, and the sensitizer Yb^{3+} effectively enhances the UC luminescence intensity because of the efficient energy transfer from Yb^{3+} to Ho^{3+}. The UC intensity is dependent on the Yb^{3+}:Ho^{3+} ratio in the samples 7:1 for $NaGd_{0.60}(MoO_4)_2$:$Ho_{0.05}Yb_{0.35}$, 8:1 for $NaGd_{0.55}(MoO_4)_2$:$Ho_{0.05}Yb_{0.40}$, 9:1 for $NaGd_{0.50}(MoO_4)_2$:$Ho_{0.05}Yb_{0.45}$, and 10:1 for $NaGd_{0.45}(MoO_4)_2$:$Ho_{0.05}Yb_{0.50}$. The higher intensity of $NaGd_{0.50}(MoO_4)_2$:$Ho_{0.05}Yb_{0.45}$ causes the ratio of Yb^{3+}:Ho^{3+} to be 9:1. The higher contents of Yb^{3+} ions, used as a sensitizer owing to its strong absorption at approximately 980 nm, can remarkably enhance the UC luminescence through energy transfer. The concentration quenching effect can be explained by the energy transfer between the nearest Ho^{3+} and Yb^{3+} ions. With increasing Ho^{3+} and Yb^{3+} ion concentrations, the distance between Ho^{3+} and Yb^{3+} ions decreases, which can promote non-radiative energy transfers such as exchange interactions or multipole-multipole interactions [33]. The concentration quenching of UC emissions can be mainly attributed to the different doping ions [36]. As shown in Fig. 3, the higher intensity of $NaGd_{0.50}(MoO_4)_2$:$Ho_{0.05}Yb_{0.45}$ causes the ratio of Yb^{3+}:Ho^{3+} to be 9:1, while the lower intensity of $NaGd_{0.60}(MoO_4)_2$:$Ho_{0.05}Yb_{0.35}$ causes the ratio of Yb^{3+}:Ho^{3+} to be 7:1. The optimal Yb^{3+}:Ho^{3+} ratio of 9:1 is assumed to be induced by the concentration quenching effect of Ho^{3+} ion. Therefore, a higher content of the Yb^{3+} ions used as the sensitizer and a lower content of the Ho^{3+} ions, for the correct ratio of Yb^{3+}:Ho^{3+} (9:1), can remarkably enhance the UC luminescence through efficient energy transfer.

The logarithmic scale dependence of the UC emission intensities at 545 and 655 nm on the working pump power in the range of 20 to 110 mW in the $NaGd_{0.50}(MoO_4)_2$:$Ho_{0.05}Yb_{0.45}$ sample is shown in Fig. 4. In the UC process, the UC emission intensity is proportional to the slope value n of the irradiation pumping power, where n is the number of pumped photons required to produce UC emissions [34]:

$$I \propto P^n \quad (1)$$

$$\mathrm{Ln}I \propto n\mathrm{Ln}P \quad (2)$$

where the value n is the number of pumped photons required to excite the upper emitting state, I is the UC luminescent intensity and P is the laser pumping power. The calculated slope values n in Fig. 4 indicate that the slope n is 1.85 for green emission at 545 nm; this value is 1.96 for red emission at 655 nm. These results show that the UC mechanism of the green and red emissions can be explained by a two-photon UC process in the Er^{+3}/Yb^{3+} co-doped phosphors [35,36]

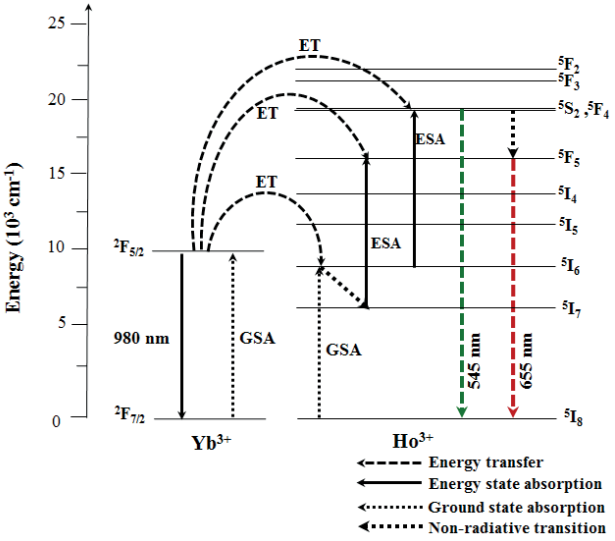

Fig. 5. Schematic energy level diagrams of Yb^{3+} (sensitizer) and Ho^{3+} ions (activator) ions in the $NaGd_{1-x}(MoO_4)_2$:Ho^{3+}/Yb^{3+} system and the upconversion mechanisms of the green and red emissions under 980 nm laser excitation.

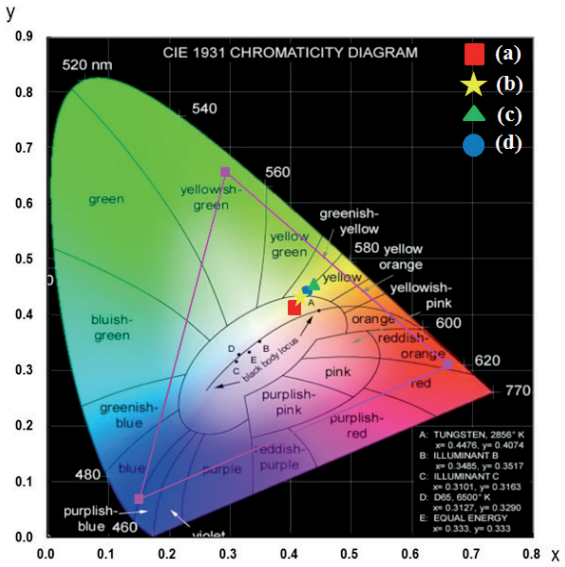

Fig. 6. CIE chromaticity diagram showing the color co-ordinates of the $NaGd_{1-x}(MoO_4)_2$:Ho^{3+}/Yb^{3+} phosphors. The inset shows the yellow emissions for the synthesized samples: (a) $NaGd_{0.60}(MoO_4)_2$:$Ho_{0.05}Yb_{0.35}$, (b) $NaGd_{0.55}(MoO_4)_2$:$Ho_{0.05}Yb_{0.40}$, (c) $NaGd_{0.50}(MoO_4)_2$:$Ho_{0.05}Yb_{0.45}$, and (d) $NaGd_{0.45}(MoO_4)_2$:$Ho_{0.05}Yb_{0.50}$.

as well as in the Ho^{+3}/Yb^{3+} co-doped phosphors [4,12,37,38].

Based on the results of the analysis of pump-power dependence, the known schematic energy level diagrams of Ho^{3+} (activator) and Yb^{3+} (sensitizer) ions in the as-prepared $NaGd_{1-x}(MoO_4)_2$ samples and the UC mechanisms, which account for the green and red emissions during 980 nm laser excitation, are shown in Fig. 5. The UC emissions are generated by a two photon process of excited state absorption (ESA) and energy transfer (ET). Initially, the Yb^{3+} ion sensitizer is excited from the $^2F_{7/2}$ level to the $^2F_{5/2}$ level under excitation of 980 nm pumping, and transfers its energy to the Ho^{3+} ions. Then, the Ho^{3+} ions are populated from the $^5I_8$ ground state to the $^5I_6$ excited state. This is a phonon-assisted energy transfer process because of the energy mismatch between the $^2F_{5/2}$ level of Yb^{3+} and the $^5I_6$ level of Ho^{3+}. Second, the Ho^{3+} in the $^5I_6$ level is excited to the $^5S_2$ or $^5F_4$ level by the next energy transfer from Yb^{3+}. In addition, the $^5S_2$ /$^5F_4$ level of Ho^{3+} can be populated through the excited state absorption. Finally, the green emission at approximately 545 nm, corresponding to the $^5S_2$/$^5F_4$ → $^5I_8$ transition, takes place. For the red emission, the population of the $^5F_5$ level is generated by two different channels. One channel is the result of Ho^{3+} in the $^5S_2$/$^5F_4$ level state relaxing non-radiatively to the $^5F_5$ level. The other channel is closely related to the $^5I_7$ level populated by non-radiative relaxation from the $^5I_6$ excited state. The Ho^{3+} in the $^5I_7$ level is excited to the $^5F_5$ level by the energy transfer from Yb^{3+} and relaxed to the $^5F_5$ level. Therefore, the red emission around 655 nm corresponds to the $^5F_5$ → $^5I_8$ transition [4,12,37,38].

Figure 6 shows the CIE chromaticity diagram for the color coordinates of the $NaGd_{1-x}(MoO_4)_2$ phosphors. The inserts indicate the chromaticity points for the samples $NaGd_{0.60}(MoO_4)_2$:$Ho_{0.05}Yb_{0.35}$, $NaGd_{0.55}(MoO_4)_2$:$Ho_{0.05}Yb_{0.40}$, $NaGd_{0.50}(MoO_4)_2$:$Ho_{0.05}Yb_{0.45}$, and $NaGd_{0.45}(MoO_4)_2$:$Ho_{0.05}Yb_{0.50}$ particles. When the concentration ratio of Yb^{3+}:Ho^{3+} is modulated, the chromaticity coordinate values (x, y) changed. The yellow emission color coordinates of the samples are well matched with the standard equal energy point. This result indicates the achievement of attractive yellow UC emissions for use as potentially active components in new optoelectronic devices and luminescent devices.

Figures 7(a)~(e) shows the Raman spectra of the synthesized pure $NaGd(MoO_4)_2$, $NaGd_{0.60}(MoO_4)_2$:$Ho_{0.05}Yb_{0.35}$, $NaGd_{0.55}(MoO_4)_2$:$Ho_{0.05}Yb_{0.40}$, $NaGd_{0.50}(MoO_4)_2$:$Ho_{0.05}Yb_{0.45}$, and $NaGd_{0.45}(MoO_4)_2$:

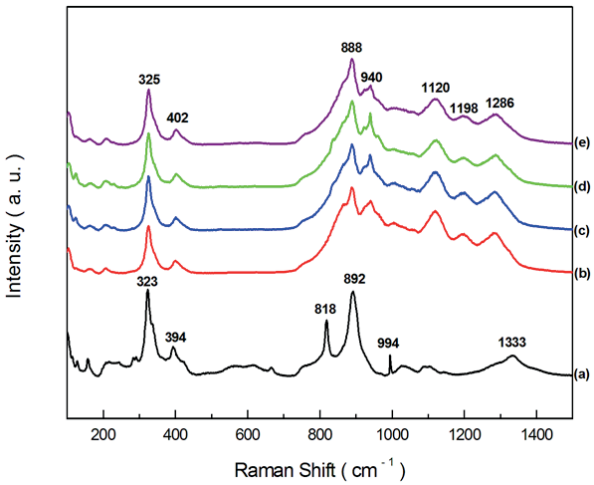

Fig. 7. Raman spectra of the synthesized (a) pure $NaGd_2(MoO_4)_4$, (b) $NaGd_{0.60}(MoO_4)_2$:$Ho_{0.05}Yb_{0.35}$, (c) $NaGd_{0.55}(MoO_4)_2$:$Ho_{0.05}Yb_{0.40}$, (d) $NaGd_{0.50}(MoO_4)_2$:$Ho_{0.05}Yb_{0.45}$, and (e) $NaGd_{0.45}(MoO_4)_2$:$Ho_{0.05}Yb_{0.50}$ particles, excited by the 514.5 nm line of an Ar ion laser at 0.5 mW.

$Ho_{0.05}Yb_{0.50}$ particles excited by the 514.5 nm line of an Ar ion laser at 0.5 mW. The internal modes for the pure $NaGd(MoO_4)_2$ particles were detected at 330, 384, 818, 892, 994 and 1,333 cm^{-1}. The well-resolved sharp peaks for $NaGd(MoO_4)_2$ indicate the high crystallinity state of the synthesized particles. The internal vibration mode frequencies are dependent on the lattice parameters and the strength of the partially covalent bond between the cation and the molecular ionic group MoO_4. The Raman spectrum of the $NaGd(MoO_4)_2$ crystal in Fig. 7(a) is that of the typical molybdate compounds, and is divided into two parts with a wide empty gap of 400-800 cm^{-1}. The highest intensity of the wavenumber band at 892 cm^{-1} corresponds to the stretching vibrations of the MoO_4. Stretching vibrations of Mo-O bonds are observed at the 818 cm^{-1} regions. For these stretching vibrations, strong mixing occurs between the Mo-O bonds and the MoO_4. The band at 323 and 394 cm^{-1} may have originated from

vibrations of the longer Mo-O bonds, which are employed in the formation of the Mo-Mo bridge.

The Raman spectra of $NaGd_{0.60}(MoO_4)_2$:$Ho_{0.05}Yb_{0.35}$, $NaGd_{0.55}(MoO_4)_2$:$Ho_{0.05}Yb_{0.40}$, $NaGd_{0.50}(MoO_4)_2$:$Ho_{0.05}Yb_{0.45}$, and $NaGd_{0.45}(MoO_4)_2$:$Ho_{0.05}Yb_{0.50}$ particles indicate very strong and dominant peaks at higher frequencies of 888, 940, 1,120, 1,198 and 1,286 cm^{-1} and at lower frequencies of 326 and 402 cm^{-1}. The strong disordered peaks at higher frequencies are attributed to the formation of modulated structures of $NaGd_{1-x}(MoO_4)_2$ due to the strong mixing between the Mo-O bonds and the MoO_4 stretching vibrations by the incorporation of the Ho^{3+} and Yb^{3+} elements into the crystal lattice, which result in the unit cell shrinkage that accompanies the highly modulated MoO_{4-x} group. These incommensurately modulated structures were also observed in several molybdate and tungstate compounds [39-41]. Previously, our research group had reported on this strongly dominant spectra of the incommensurately modulated structure in the case of $CaGd_2(MO_4)_4$:Ho^{3+}/Yb^{3+} phosphors [42]. It should be emphasized that the doped samples under excitation at 514.5 nm are superimposed because of strong Ho^{3+} luminescence lines and strongly affected by the concentration quenching effect of Ho^{3+} ions. These results, which can overcome the current limitations of traditional photoluminescence materials, can be considered to indicate that these materials have the potential for use as active components in new optoelectronic devices and in luminescent imaging.

4. CONCLUSIONS

Double molybdate $NaGd_{1-x}(MoO_4)_2$:Ho^{3+}/Yb^{3+} UC phosphors with proper doping concentrations of Ho^{3+} and Yb^{3+} were successfully synthesized using the microwave sol-gel method. Well-crystallized particles formed after heat-treatment at 800℃ for 16 h showed fine and homogeneous morphology with particle sizes of 1~3 μm. Under excitation at 980 nm, the UC doped particles exhibited yellow emissions based on a strong 545 nm emission band in the green region and a very strong 655 nm emission band in the red region, which were assigned to the $^5S_2/^5F_4 \rightarrow {}^5I_8$ and $^5F_5 \rightarrow {}^5I_8$ transitions, respectively. Higher intensity of $NaGd_{0.50}(MoO_4)_2$:$Ho_{0.05}Yb_{0.45}$ indicated that the ratio of Yb^{3+}:Ho^{3+} would be 9:1, wherein the higher contents of Yb^{3+} ion as a sensitizer could remarkably enhance the UC luminescence through energy transfer, owing to its absorption around 980 nm. The calculated slope values *n* indicate a slope $n = 1.85$ for green emission at 545 nm and a slope $n = 1.96$ for red emission at 655 nm. The yellow emission color coordinates of the samples were well-matched with the standard equal energy point. These results indicated the achievement of attractive yellow UC emissions for use as potentially active components in new optoelectronic devices and luminescent devices**.**

ACKNOWLEDGMENT

This study was supported by the Research Program through the Campus Research Foundation funded by Hanseo University in 2017 (171Egong07).

REFERENCES

[1] M. V. DaCosta, S. Doughan, Y. Han, and U. J. Krull, *Anal. Chim. Acta*, **832**, 1 (2014). [DOI: https://doi.org/10.1016/j.aca.2014.04.030]

[2] M. Lin, Y. Zho, S. Q. Wang, M, Liu, Z. F. Duan, Y. M. Chen, F. Li, F. Xu, and T. J. Lu, *Biotechnol. Adv.*, **30**, 1551 (2012). [DOI: https://doi.org/10.1016/j.biotechadv.2012.04.009]

[3] M. Wang, G. Abbineni, A. Clevenger, C. Mao, and S. Xu, *Nanomed.: Nanotech. Biol. Med.*, **7**, 710 (2011).

[4] C. S. Lim, A. Aleksandrovsky, M. Molokeev, A. Oreshonkov, and V. Atuchin, *Phys. Chem. Chem. Phys.*, **17**, 19278 (2015). [DOI: https://doi.org/10.1039/C5CP03054D]

[5] C. S. Lim, *Mater. Res. Bull.*, **75**, 211 (2016). [DOI: https://doi.org/10.1016/j.materresbull.2015.11.058]

[6] L. Li, L. Liu, W. Zi, H. Yu, S. Gan, G. Ji, H. Zou, and X. Xu, *J. Lumin.*, **143**, 14 (2013). [DOI: https://doi.org/10.1016/j.jlumin.2013.04.031]

[7] C. Ming, F. Song, and L. Yan, *Opt. Commun.*, **286**, 217 (2013). [DOI: https://doi.org/10.1016/j.optcom.2012.08.095]

[8] N. Xue, X. Fan, Z. Wang, and M. Wang, *J. Phys. Chem. Sol.*, **69**, 1891 (2008). [DOI: https://doi.org/10.1016/j.jpcs.2008.01.015]

[9] Z. Shan, D. Chen, Y. Yu, P. Huang, F. Weng, H. Lin, and Y. Wang, *Mater. Res. Bull.*, **45**, 1017 (2010). [DOI: https://doi.org/10.1016/j.materresbull.2010.04.004]

[10] W. Liu, J. Sun, X. Li, J. Zhang, Y. Tian, S. Fu, H. Zhong, T. Liu, L. Cheng, H. Zhong, H. Xia, B. Dong, R. Hua, X. Zhang, and B. Chen, *Opt. Mater.*, **35**, 1487 (2013). [DOI: https://doi.org/10.1016/j.optmat.2013.03.008]

[11] W. Xu, H. Zhao, Y. Li, L. Zheng, Z. Zhang, and W. Cao, *Sensors and Act. B: Chem.*, **188**, 1096 (2013). [DOI: https://doi.org/10.1016/j.snb.2013.07.094]

[12] J. Tang, C. Cheng, Y. Chen, and Y. Huang, *J. Alloys Compd.*, **609**, 268 (2014). [DOI: https://doi.org/10.1016/j.jallcom.2014.04.134]

[13] W. Zhang, J. Li, Y. Wang, J. Long, and K. Qiu, *J. Alloys Compd.*, **635**, 16 (2015). [DOI: https://doi.org/10.1016/j.jallcom.2015.02.106]

[14] F. Mo, L. Zhou, Q. Pang, F. Gong, and Z. Liang, *Ceram. Inter.*, **38**, 6289 (2012). [DOI: https://doi.org/10.1016/j.ceramint.2012.04.084]

[15] G. Li, S. Lan, L. Li, M. Li, W. Bao, H. Zou, X. Xu, and S. Gan, *J. Alloys Compd.*, **513**, 145 (2012). [DOI: https://doi.org/10.1016/j.jallcom.2011.10.008]

[16] J. Liao, H. Huang, H. You, X. Qiu, Y. Li, B. Qiu, and H. R. Wen, *Mater. Res. Bull.*, **45**, 1145 (2010). [DOI: https://doi.org/10.1016/j.materresbull.2010.05.027]

[17] F. B. Cao, L. S. Li, Y. W. Tian, and X. R. Wu, *Optics Laser Tech.*, **55**, 6 (2014). [DOI: https://doi.org/10.1016/j.optlastec.2013.06.016]

[18] G. M. Kuz'micheva, D. A. Lis, K. A. Subbotin, V. B. Rybakov, and E. V. Zharikov, *J. Crys. Growth*, **275**, e1835 (2005).

[19] X. Lu, Z. You, J. Li, Z. Zhu, G. Jia, B. Wu, and C. Tu, *J. Alloys Compd.*, **458**, 462 (2008). [DOI: https://doi.org/10.1016/j.jallcom.2007.04.010]

[20] X. Li, Z. Lin, L. Zhang, and G. Wang, *J. Crys. Growth*, **290**, 670 (2006). [DOI: https://doi.org/10.1016/j.jcrysgro.2006.02.005]

[21] Y. K. Voron'ko, K. A. Subbotin, V. E. Shukshin, D. A. Lis, S. N. Ushakov, A. V. Popov, and E. V. Zharikov, *Opt. Mater.*, **29**, 246 (2009).

[22] H. Lin, X. Yan, and X. Wang, *J. Sol. State. Chem.*, **204**, 266 (2013). [DOI: https://doi.org/10.1016/j.jssc.2013.06.020]

[23] G. Li, L. Li, M. Li, W. Bao, Y. Song, S. Gan, H. Zou, and X. Xu, *J. Alloys Compd.*, **550**, 1 (2013). [DOI: https://doi.org/10.1016/j.jallcom.2012.09.125]

[24] Y. Huang, L. Zhou, L. Yang, and Z. Tang, *Opt. Mater.*, **33**, 777 (2011). [DOI: https://doi.org/10.1016/j.optmat.2010.12.015]

[25] L. Li, W. Zi, G. Li, S. Lan, G. Ji, S. Gan, H. Zou, and X. Xu, *J. Sol. State Chem.*, **191**, 175 (2012). [DOI: https://doi.org/10.1016/j.jssc.2012.03.003]

[26] Y. Tian, B. Chen, B. Tian, J. Sun, X. Li, J. Zhang, L. Cheng, H. Zhong, H. Zhong, Q. Meng, and R. Hua, *Physica B.*, **407**, 2556 (2012). [DOI: https://doi.org/10.1016/j.physb.2012.03.066]

[27] J. Zhang, X. Wang, X. Zhang, X. Zhao, X. Liu, and L. Peng, *Inorg. Chem. Commun.*, **14**, 1723 (2011). [DOI: https://doi.org/10.1016/j.inoche.2011.07.015]

[28] S. W. Park, B. K. Moon, B. C. Choi, J. H. Jeong, J. S. Bae, and K. H. Kim, *Curr. Appl. Phys.*, **12**, S150 (2012).

[29] C. S. Lim, *Mater. Res. Bull.*, **47**, 4220 (2012). [DOI: https://doi.org/10.1016/j.materresbull.2012.09.029]

[30] C. S. Lim, *Mater. Chem. Phys.*, **131**, 714 (2012). [DOI: https://doi.org/10.1016/j.matchemphys.2011.10.039]

[31] C. S. Lim, *Infrar. Phys. Tech.*, **67**, 371 (2014). [DOI: https://doi.org/10.1016/j.infrared.2014.08.018]

[32] R. D. Shanan, *Acta Cryst.*, **A32**, 751 (1976).

[33] F. Anzel, G. Baldacchini, L. Laversenne, and G. Boulon, *Opt. Mat.*, **24**, 103

(2003). [DOI: https://doi.org/10.1016/S0925-3467(03)00112-5]
[34] H. Guo, N. Dong, M. Yin, W. Zhang, L. Lou, and S. Xia, *J. Phys. Chem. B*, **108**, 19205 (2004). [DOI: https://doi.org/10.1021/jp048072q]
[35] H. Du, Y. Lan, Z. Xia, and J. Sun, *Mater Res. Bull.*, **44**, 1660 (2009). [DOI: https://doi.org/10.1016/j.materresbull.2009.04.009]
[36] W. Lu, L. Cheng, J. Sun, H. Zhong, X. Li, Y. Tian, J. Wan, Y. Zheng, L. Huang, T. Yu, H. Yu, and B. Chen, *Physica B*, **405**, 3284 (2010). [DOI: https://doi.org/10.1016/j.physb.2010.04.061]
[37] C. S. Lim, *Ceram. Inter.*, **41**, 2616 (2015). [DOI: https://doi.org/10.1016/j.ceramint.2015.06.052]
[38] C. S. Lim, *J. Phys. Chem. Sol.*, **76**, 65 (2015).
[39] A. M. Abakumov, V. A. Morozov, A. A. Tsirlin, J. Verbeeck, and J. Hadermann, *Inorg. Chem.*, **53**, 9407 (2014). [DOI: https://doi.org/10.1021/ic5015412]
[40] V. A. Morozov, A. Bertha, K. W. Meert, S. Van Rompaey, D. Batuk, G. T. Martinez, S. Van Aert, P. F. Smet, M. V. Raskina, D. Poelman, A. M. Abakumov, and J. Hadermann, *Chem. Mat.*, **25**, 4387 (2013). [DOI: https://doi.org/10.1021/cm402729r]
[41] V. A. Morozov, A. V. Mironov, B. I. Lazoryak. E. G. Khaikina, O. M. Basovich, M. D. Rossell, and G. V. Tendeloo, *J. Solid State Chem.*, **179**, 1183 (2006). [DOI: https://doi.org/10.1016/j.jssc.2005.12.041]
[42] C. S. Lim, V. V. Atuchin, A. S. Aleksandrovsky, M. S. Molokeev, and A. S. Oreshonkov, *J. Alloys Compd.*, **695**, 737 (2017). [DOI: https://doi.org/10.1016/j.jallcom. 2016.06.134]